

We are IntechOpen, the world's leading publisher of Open Access books Built by scientists, for scientists

6,900

Open access books available

185,000

International authors and editors

200M

Downloads

Our authors are among the

154

Countries delivered to

TOP 1%

most cited scientists

12.2%

Contributors from top 500 universities



WEB OF SCIENCE™

Selection of our books indexed in the Book Citation Index
in Web of Science™ Core Collection (BKCI)

Interested in publishing with us?
Contact book.department@intechopen.com

Numbers displayed above are based on latest data collected.
For more information visit www.intechopen.com



Kinematics: On Direction Cosine Matrices

Brendon Smeresky and Alex Rizzo

Abstract

Motion mechanics (dynamics) comprises kinetics to describe the implications of applied forces and torques; and also kinematics (phoronomics). Developed in the 1700s, kinematics describes mathematical translations from one basis of measurement to another using common kinematic measurement variables like quaternions, Euler angles, and direction cosine matrices. Two ubiquitous rotation sequences are unquestionably adopted for developing modern direction cosine matrices from among the 12 potential options, stemming from applicability to aerospace systems, accuracy, and computation burden. This chapter provides a comprehensive reevaluation of all 12 options yielding a menu of options for accuracy and computational burdens, with the results illustrated compared to the ubiquitous two modernly adopted choices, broken into two rotational groups: symmetric rotations and nonsymmetric rotations. Validation will be provided by critical analysis of integration using step size to illustrate correlated minimal accuracy. No single rotational sequence is universally superior with respect to all figures of merit, enabling trade-space analysis between rotational sequences. One interesting revelation of one of the two ubiquitous sequences (the 3-1-3 symmetric sequence) is illustrated to have relatively less accuracy but lower computational burden than the other (the 3-2-1 nonsymmetric sequence). Meanwhile, a relatively unknown “2-3-1” rotational sequence is shown to have similar computational burden and accuracy.

Keywords: phoronomics, mechanics, kinetics, kinematics, direction cosines, Euler angles, space dynamics, digital computation, control systems, control engineering

1. Introduction

In 1775, Leonhard Euler developed motion phoronomics [1] which immediately blossomed in the next two centuries [2–29]. The space race between the now-defunct Soviet Union and the United State of the last century gave substantial impetus to development and adoption of motion kinematics together with survival imperatives driven by the nuclear cold war. The resultant lineage of literature contains seemingly countless technical and non-technical [30–62]. With this heritage the two most common rotational sequences used to calculate direction cosine matrices are referred to as “aerospace” sequences for nonsymmetric sequences (where the resulting angles are referred to as Tait-Bryan angles), while the symmetric sequences are oft referred to as “orbital” sequences (where the resulting angles are called proper “Euler Angles”) [63].

In light of continued improvement in computational capabilities, the focus of this research is to evaluate all 12 rotation sequences comparing by mean and standard deviation of accuracy reflecting roll, pitch, and yaw angles; and also comparing by computational burden embodies by time required to perform the calculations. The chapter questions whether the 3-2-1 rotational sequence truly the best with respect to either of these figures of merit (statistical accuracy and computational burden). The results illustrate the two standard sequences are indeed good (with relative weaknesses). In particular the standard asymmetric sequence is more accurate, but slower than the standard symmetric sequence. On average, despite fewer mathematical steps, the symmetric rotations are on average slower to calculate. The 3-2-1 sequence is quickest to calculate amongst the asymmetric rotations, meanwhile the 2-3-2 and 1-2-1 are the quickest amongst the symmetric rotations.

Artificial intelligence and machine learning has evidenced the need for rapid calculations, so as motion mechanics incorporate adopt these new learning algorithms, the impact of this chapter become increasingly relevant in that options revealed in here illustrate simultaneous accuracy and favorable rapidity of calculation [62]. This chapter also complements other algorithmic advances [37–45] like system identification [55–59] including nonlinear adaptive forms and also control [46–54] for space guidance, navigation, and control (GNC) missions [35, 36, 60–65] in a time when the United States is developing and relying upon more advanced Machine Learning and AI products than ever before.

2. Materials and methods

One application of motion mechanics is the control of the attitude of spacecraft rotational maneuvers or even maintenance of a specified attitude. The key reminder is that Euler’s moment equations governing rotational movement apply in a non-moving reference frame referred to as “inertial,” which is a reference frame that has no meaning as a basis for measurement (i.e., it is not possible to identify a truly non-moving reference frame that can be used for measurement of angular position). This section of the chapter illustrates the method to numerically evaluate the options for kinematic expressions of rotations between chosen frames of reference (e.g., the body frame) and the inertial frame. MATLAB/SIMULINK depicted in **Figure 1** is used to create a simulation of rotation of spacecraft and necessary components of the simulation to make it relatively high-fidelity include aerodynamic and gravity gradient disturbances; kinematic expressions including quaternions, direction cosine matrices, and Euler angles; and even incorporation of the

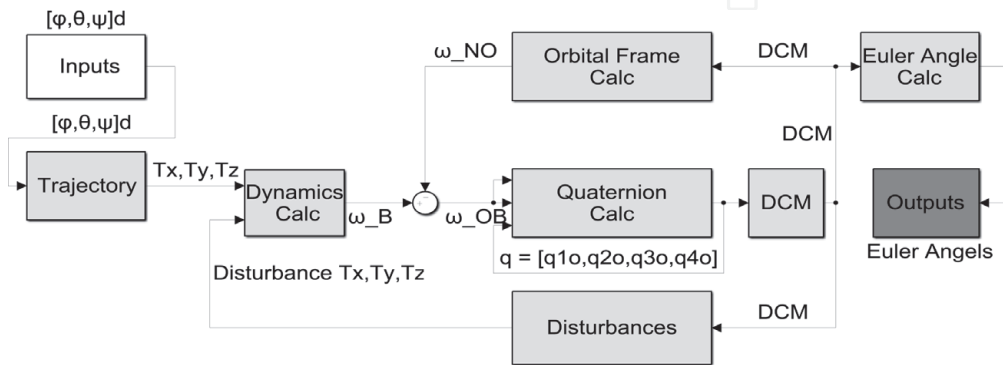


Figure 1. MATLAB/SIMULINK simulation where controllers (not articulated) are fed a full-state trajectory autonomously generated, while the resulting motion is expressed in various forms of kinematics establishing the attitude that results in a specific calculations of disturbance torques.

motion of an object in a specified orbit. The simulation is elaborated in Section 2, while Section 3 will describe the experiments, with concluding results in Section 4.

2.1 Theory of dynamics

Mechanics and dynamics are synonyms. Interestingly, kinematics (which is also currently called phoronomics [13]) was referred to as “statics” in the era of Newton [2] indicating the lack of motion which is included in kinetics. This will be elaborated further in Section 2.1.2. Michael Chasle’s theorems permit us to simply “invoke” Euler’s moment equation to describe three-degrees of rotation and Newton’s law to describe three-degrees of translation; together comprising a full mathematical description of so-called 6DOF motion, or motion in six-degrees. Euler describes rotational motion expressed in a moving body frame as $T = J\dot{\omega} + \omega \times J\omega$ [6], where $[J]$ is a matrix of mass moments of inertia explained by Kane [23]. Measurements of rotational maneuvers are expressed in inertial coordinates by establishing an arbitrarily placed inertial reference frame $[X_I, Y_I, Z_I]$, while kinematics relate the inertial coordinates to those expressed in the body reference frame $[X_B, Y_B, Z_B]$. References in the literature use the nomenclature “direction cosine matrix” [18], since the matrix is composed of projection components, where the dot-product projection operation is defined by the cosine of the angle between the two reference frames [17, 25, 26]. Individual vector components elaborate the orientation angle between reference frames [28].

2.1.1 Kinetics

Kinetics, or Dynamics, is the process of describing the motion of objects with focus on the forces involved. In the inertial frame, Newton’s $F = ma$ is applied but becomes Euler’s $T = J\dot{\omega}$ when rotation is added, where $T = J\dot{\omega}$ is expressed in the inertial reference frame’s coordinates, while $T = J\dot{\omega} + \omega \times J\omega$ from above is still measured in the inertial frame, but expressed in body coordinates.

Combining the Euler and Newton equations, we can account for all six degrees of freedom. In application, when an input angle $[\varphi_d, \theta_d, \psi_d]$ is commanded, the feedforward control uses Eq. (1) as the ideal controller with Eq. (2) as the sinusoidal trajectory to calculate the required torque $[T_x, T_y, T_z]$ necessary to achieve the desired input angle. The Dynamics calculator then uses Eq. (3) to convert the torques into ω_B values, where ω_B is defined as the angular velocity of the body. In order to calculate this, the non-diagonal terms in Eq. (4) are neglected, removing coupled motion and leaving only the principle moments of inertia. Then, the inertia matrix J is removed from $\dot{\omega}$, and the remaining $\dot{\omega}$ is integrated into $[\omega_x, \omega_y, \omega_z]$, which is fed into the Kinematics block of the model to finally determine the outputted Euler Angles.

$$T_d = J\dot{\omega}_d + \omega_d \times J\omega_d \quad (1)$$

$$\theta = \frac{1}{2} (A + A \sin(\omega_f t + \varphi)) \quad (2)$$

$$T = \dot{H}_i = J\dot{\omega}_i + \omega_i \times J\omega_i \quad (3)$$

2.1.2 Kinematics, phoronomics, or “The Laws of Going”

Formulation of spacecraft attitude dynamics and control problems involves considerations of kinematics, especially as it pertains to the orientation of a rigid body that is in rotational motion. The subject of kinematics is mathematical in nature, because it does not involve any forces associated with motion. The kinematic

representation of the orientation of one reference frame relative to another reference can also be expressed by introducing the time-dependence of Euler Angles. The so-called body-axis rotations involve successive rotations three times about the axes of the rotated body-fixed reference frame resulting in 12 possible sets of Euler angles. The so-called space-axis rotations instead involve three successive rotations using axes fixed in the inertial frame of reference, again producing 12 possible sets of Euler angles. Because the body-axis and space-axis rotations are intimately related, only 12 Euler angle possibilities need be investigated; and the 12 sets from the body-axis sequence are typically used [26]. Consider a rigid body fixed at a stationary point whose inertia ellipsoid at the origin is an ellipsoid of revolution whose center of gravity lies on the axis of symmetry. Rotation around the axis of symmetry does not change the Lagrangian function, so there must-exist a first integral which is a projection of an angular momentum vector onto the axis of symmetry. Three coordinates in the configuration space special orthogonal group (3) may be used to form a local coordinate system, and these coordinates are called the Euler angles.

Key tools of kinematics from which the Euler angles may be derived include direction cosines which describe orientation of the body set of axes relative to an external set of axes. Euler's angles may be defined by the following set of rotations: "rotation about x axis by angle θ , rotation about z' axis by an angle ψ , then rotation about the original z-axis by angle ϕ ". Eulerian angles have several "conventions: Goldstein uses [22] the "x-convention": z-rotation followed by x' rotation, followed by z' rotation (essentially a 3-1-3 sequence). Quantum mechanics, nuclear physics, and particle physics the "y-convention" is used: essentially a 3-2-3 rotation. Both of these have drawbacks, that the primed coordinate system is only slightly different than the unprimed system, such that, ϕ and ψ become indistinguishable, since their respective axes of rotation (z and z') are nearly coincident. The so-called Tait-Bryan convention in **Figure 2** therefore gets around this problem by making each of the three rotations about different axes: (essentially a 3-2-1 sequence) [22].

Kinematics is the process of describing the motion of objects without focus on the forces involved. The $[\omega_x, \omega_y, \omega_z]$ values from the Dynamics are fed into the Quaternion Calculator where Eqs. (5) and (6) yield q , the Quaternion vector. The Quaternions define the Euler axis in three dimensional space using $[q_1, q_2, q_3]$. About this axis, a single angle of rotation $[q_4]$ can resolve an object aligned in reference frame A into reference frame B. The Direction Cosine Matrix (DCM) then relates the input ω values to the Euler Angles using one of 12 permutations of possible rotation sequences, where multiple rotations can be made in sequence. Therefore, the rows of

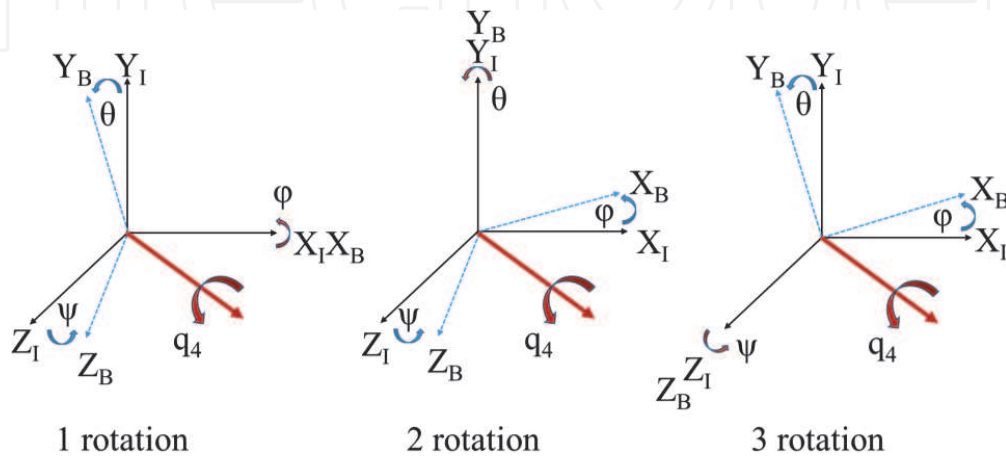


Figure 2. Execution of a 3-2-1 rotation from CA to CB (left to right); blue-dotted arrows denote angle rotations. A direct rotation from CA to CB can be made about the Euler Axis, q_4 in red. The set of three rotations may be depicted as four rectangular parallelepipeds, where each contains the unit vectors of the corresponding reference frame [29].

the DCM show the axes of Frame A represented in Frame B, the columns show the axes of Frame B represented in Frame A, and φ , θ , and ψ are the angles of rotation that must occur in each axis sequentially to rotate from orientation A to orientation B, turning C^A to C^B . **Figure 2** depicts a 3-2-1 sequence to rotate from C^A to C^B , where the Euler Axis is annotated by the thickest line.

$$\begin{aligned}
 & \begin{bmatrix} J_{xx}\dot{\omega}_x + J_{xy}\dot{\omega}_y + J_{xz}\dot{\omega}_z - J_{xy}\omega_x\omega_z - J_{yy}\omega_y\omega_z - J_{yz}\omega_z^2 + J_{xz}\omega_x\omega_y + J_{zz}\omega_z\omega_y + J_{yz}\omega_y^2 \\ J_{yx}\dot{\omega}_x + J_{yy}\dot{\omega}_y + J_{yz}\dot{\omega}_z - J_{yz}\omega_x\omega_y - J_{zz}\omega_x\omega_z - J_{xz}\omega_x^2 + J_{xx}\omega_x\omega_z + J_{xy}\omega_z\omega_y + J_{xz}\omega_z^2 \\ J_{zx}\dot{\omega}_x + J_{zy}\dot{\omega}_y + J_{zz}\dot{\omega}_z - J_{xx}\omega_x\omega_y - J_{xz}\omega_y\omega_z - J_{xy}\omega_y^2 + J_{yy}\omega_x\omega_y + J_{yz}\omega_z\omega_x + J_{xy}\omega_x^2 \end{bmatrix} \\
 &= \begin{bmatrix} T_x \\ T_y \\ T_z \end{bmatrix}
 \end{aligned} \tag{4}$$

$$\begin{bmatrix} \dot{q}_1 \\ \dot{q}_2 \\ \dot{q}_3 \\ \dot{q}_4 \end{bmatrix} = \frac{1}{2} \begin{bmatrix} 0 & \omega_3 & -\omega_2 & \omega_1 \\ -\omega_3 & 0 & \omega_1 & \omega_2 \\ \omega_2 & -\omega_1 & 0 & \omega_3 \\ -\omega_1 & -\omega_2 & -\omega_3 & 0 \end{bmatrix} \begin{bmatrix} q_1 \\ q_2 \\ q_3 \\ q_4 \end{bmatrix} = \frac{1}{2} \begin{bmatrix} q_4 & -q_3 & q_2 & q_1 \\ q_3 & q_4 & -q_1 & q_2 \\ -q_2 & q_1 & q_4 & q_3 \\ -q_1 & -q_2 & -q_3 & q_4 \end{bmatrix} \begin{bmatrix} \omega_1 \\ \omega_2 \\ \omega_3 \\ 0 \end{bmatrix} \tag{5}$$

$$\begin{aligned}
 & \begin{bmatrix} 1 - 2(q_2^2 + q_3^2) & 2(q_1q_2 + q_3q_4) & 2(q_1q_3 - q_2q_4) \\ 2(q_2q_1 - q_3q_4) & 1 - 2(q_1^2 + q_3^2) & 2(q_2q_3 + q_1q_4) \\ 2(q_3q_1 + q_2q_4) & 2(q_3q_2 - q_1q_4) & 1 - 2(q_1^2 + q_2^2) \end{bmatrix} \\
 &= \begin{bmatrix} C_2C_3 & C_2S_3 & -S_2 \\ S_1S_2C_3 - C_1S_3 & S_1S_2S_3 + C_1C_3 & S_1C_2 \\ C_1S_2C_3 - S_1S_3 & C_1S_2S_3 - S_1C_3 & C_1C_2 \end{bmatrix}
 \end{aligned} \tag{6}$$

2.1.3 The orbital frame

In order to more completely represent a maneuvering spacecraft, orbital motion must be included with the Kinematics. This relationship is represented in **Figure 1**, where the output of the DCM is fed into the Orbital Frame Calculator, and the second column of the DCM is multiplied against the orbital velocity of the spacecraft. The second column of the DCM represents the Y axis of Frame B projected in the X, Y, and Z axes of Frame A. This yields ω^{NO} , the orbital velocity relative to the Inertial Frame. Using Eq. (7), this velocity is removed from the velocity of the body relative to the Inertial Frame, leaving only the velocity of the body relative to the Orbital Frame for further calculations.

$$\omega^{OB} = \omega^{NB} - \omega^{NO} \tag{7}$$

2.1.4 Disturbances

Multiple disturbance torques exist that effect the motion of a spacecraft in orbit, two of which are addressed in this paper. The first is the disturbance due to gravity acting upon an object in orbit, where the force due to gravity decreases as the

distance between objects increases. The force is applied as a scaling factor to the mass distribution around the Z axis of a spacecraft. This force applied to a mass offset from the center of gravity is calculated through the cross product found in Eq. (8) and yields an output torque about the Z axis.

The second disturbance is an aerodynamic torque due to the force of the atmosphere acting upon a spacecraft, which also decreases as the altitude increases. In Eq. (9), the force due to air resistance is calculated by scaling the direction of orbital velocity by the atmospheric density, drag coefficient, and magnitude of orbital velocity. This force then acts upon the center of pressure, which is offset from the center of gravity, and yields a torque about the Z axis, due to the cross product in Eq. (9).

The disturbances are additive and act upon the dynamics in **Figure 1**. Because the ideal feedforward controller is the dynamics, an offsetting component equal to the negative anticipated disturbances can be used to negate the disturbance torque. This results in nullifying the disturbances when the two are summed to produce ω^{OB} , the velocity of the body relative to the Inertial Frame.

$$T_g = 3 \frac{\mu}{R^3} \hat{z} \times J \hat{z} \quad (8)$$

$$T_a = C_p \times f_a = C_p \times [(\rho_a V_R^2 A_p) \hat{V}_R] \quad (9)$$

2.2 Experimental setup

A model of the 12 DCM to Euler Angle rotations was implemented in Matlab and Simulink for this experiment. A [30, 0, 0] maneuver was commanded in the $[\varphi, \theta, \psi]$ channels, respectively. The expected runtime of each scenario was 15 s, comprised of a 5 s quiescent period, a 5 s maneuver time, and a 5 s post maneuver period for observations. The maneuver was initiated using a sinusoidal trajectory, calculated with $\omega_f = \pi/2$ and $\varphi = \pi/2$.

The simulated spacecraft had an inertia matrix of $J = [2, 0.1, 0.1; 0.1, 2, 0.1; 0.1, 0.1, 2]$, the torque was initialized as $T = [0, 0, 0]$, and the quaternion was initialized as $q = [0, 0, 0, 1]$. The spacecraft was simulated to fly at an altitude of 150 km, and received a drag coefficient of 2.5. For this experiment, both orbital motion and torque disturbances were turned off in order to simplify the simulation.

The Matlab and Simulink models utilized the Runge-Kutta solver, with an ode4 back-end. Multiple step sizes were tested to determine accuracy variations for each of the rotations: 0.1, 0.001, and 0.0001 s. The trigonometric function used to mathematically solve for the Euler Angles was the atan2 function in Matlab.

Three figures of Merit were used to assess performance. The first two were the mean and standard deviation between the Euler Angles and Body Angles. The third was the calculation time for each rotation as a measure of complexity.

3. Experimental results and analysis

3.1 Euler angle calculations and post-processing

A relationship like Eq. (6) was created mathematically to relate the DCM and rotation matrices for each of the 12 rotation sequences. Then, φ, θ , and ψ were solved for, resulting in a mathematical process to determine the Euler Angles. This process was then coded in Matlab and Simulink, but the process was not perfect. Trigonometric quadrant errors caused the appearance of discontinuities from a commanded [30, 0, 0] maneuver. This artifact was resolved using post processing and further refinement of the DCM to rotation matrix derivations that correlated the 12 rotations

found in **Figure 3** into two groups of six rotations: symmetric and non-symmetric rotations. To further define the groups, symmetric rotations would be 1-2-1 or 2-3-2, while non-symmetric rotations would include 1-3-2 or 3-1-2 rotations.

3.2 Euler angle to body angle accuracy

Accuracy was measured in the experiment by measuring the difference between the Body Angles and output Euler Angles. The expectation was that a perfectly accurate system would have a difference of zero. **Figure 4** depicts the deviation over time and **Table 1** provides the associated mean values and standard deviations for each of the rotations.

The six non-symmetric rotations show consistent error in ϕ , and only begin to deviate beyond the fifth decimal place in both mean error and standard deviation.

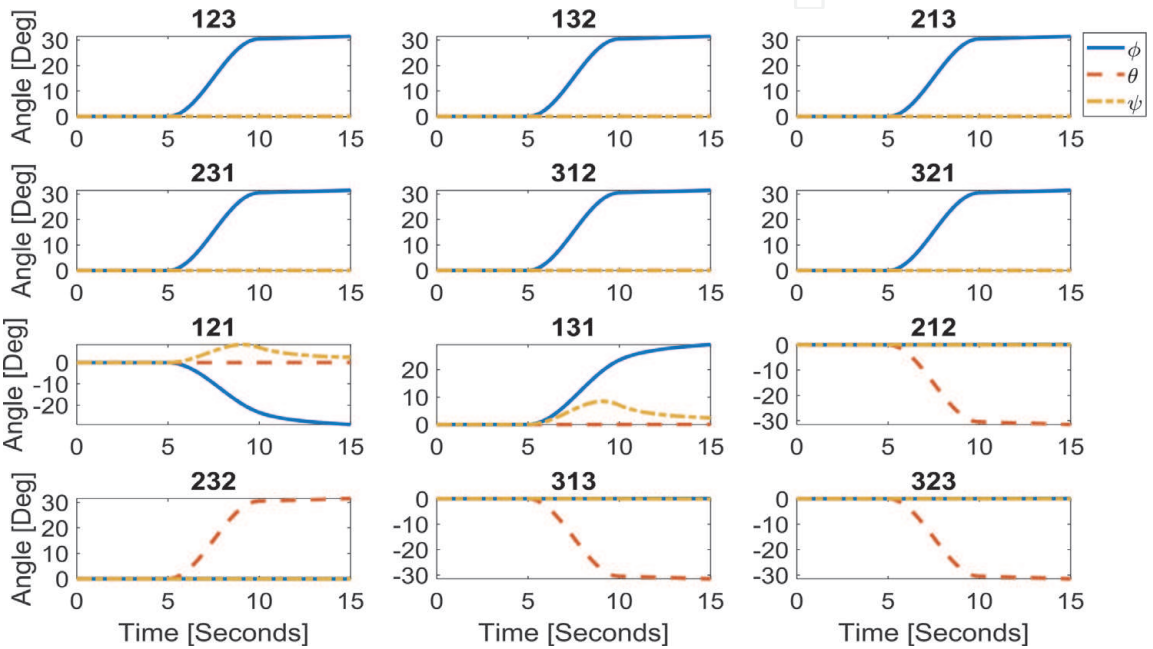


Figure 3.
Corrected Euler angles vs. time for all 12 DCM rotations.

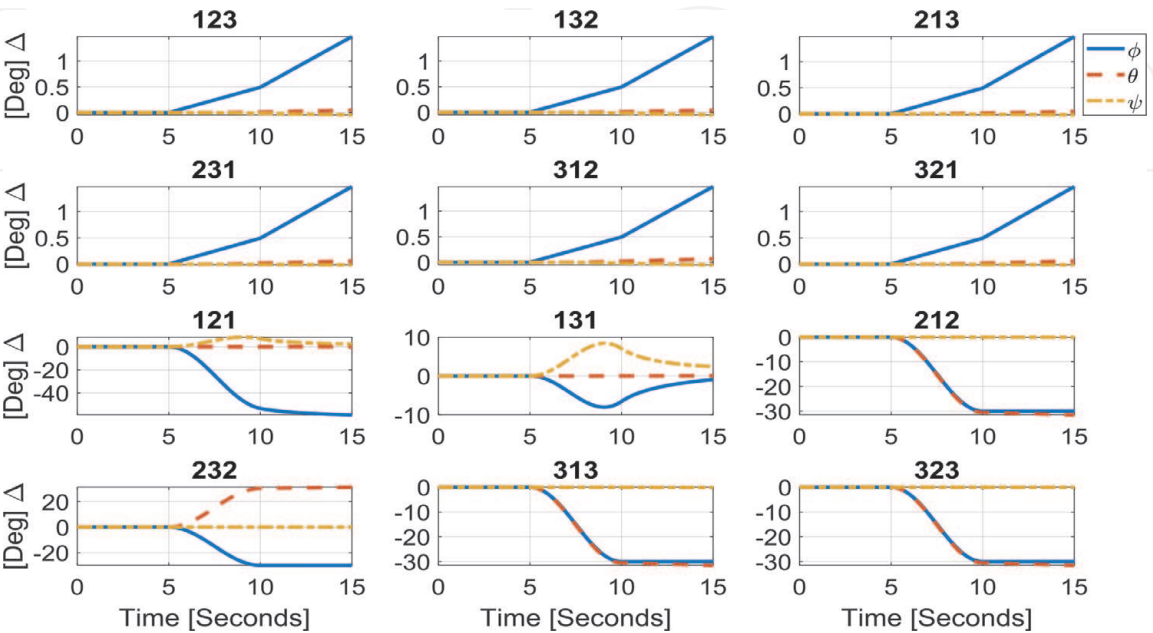


Figure 4.
Euler and body angle deviation, using a 0.1 step size.

DCM	Mean			Standard deviation		
	φ	θ	ψ	φ	θ	ψ
1-2-3	0.413	0.011	0.011	0.462	0.015	0.014
1-3-2	0.413	0.010	0.013	0.462	0.013	0.016
2-1-3	0.413	0.011	0.005	0.462	0.015	0.006
2-3-1	0.413	0.014	0.005	0.462	0.018	0.005
3-1-2	0.413	0.016	0.013	0.462	0.021	0.016
3-2-1	0.413	0.014	0.005	0.462	0.018	0.005
1-2-1	27.544	0.015	2.869	25.804	0.019	2.823
1-3-1	2.456	0.015	2.869	2.680	0.019	2.823
2-1-2	14.977	15.413	0.010	13.725	14.150	0.010
2-3-2	15.010	15.413	0.010	13.757	14.150	0.010
3-1-3	14.980	15.413	0.028	13.728	14.150	0.034
3-2-3	14.977	15.413	0.010	13.725	14.150	0.010

Table 1.
Mean and standard deviation for all 12 rotations, using a 0.1 step size.

While φ is commanded to change to 30° , θ , and ψ are expected to remain at zero, but show non-zero values due to error incurred by step size.

The six symmetric rotations are substantially harder to draw conclusions from because of the uncorrelated rotations. The mean error and standard deviation values are drastically different from each other in **Table 1** and visibly deviate in **Figure 4**. Therefore, further correlation is required to analyze accuracy. **Table 1** values were calculated over the 15 s simulation time, noting that some sequences had not reached steady-state values making their error values even larger compared to others in **Table 1** if the simulations had been run until steady state was reached.

3.3 Step size versus accuracy

This experiment implemented a variable step size to determine the accuracy delta resultant from the different step sizes. **Figure 5** depicts analysis using a step sizes of 0.001 s, which can be compared against **Figure 4**, which used a 0.1 s step size. The primary difference between **Figures 4** and **5** is the 2-order of magnitude increase of accuracy accompanying the two order of magnitude reduction in step size. A further reduction to a time step of 0.0001 s was made, with an additional order of magnitude increase in accuracy. Further reductions below this required more time than was feasible, but the trend holds that decreasing the step size increases accuracy. Furthermore, the relative accuracies between rotations held when the step sizes decreases, meaning the 1-3-2 and 3-1-2 rotations remained the most accurate.

3.4 DCM to Euler angle timing

All 12 rotation scenarios executed a maneuver within 5 s, with a standard pre and post maneuver observation period. However, actual runtimes sometimes exceeded this 15 s period; this is attributed to the complexity of the calculations and additional processes that were running at the time of the simulation. The results of each of the 12 rotations for each of three time steps are shown in **Table 2**. The simulation timing is effected by step size; therefore, the results can only be compared between

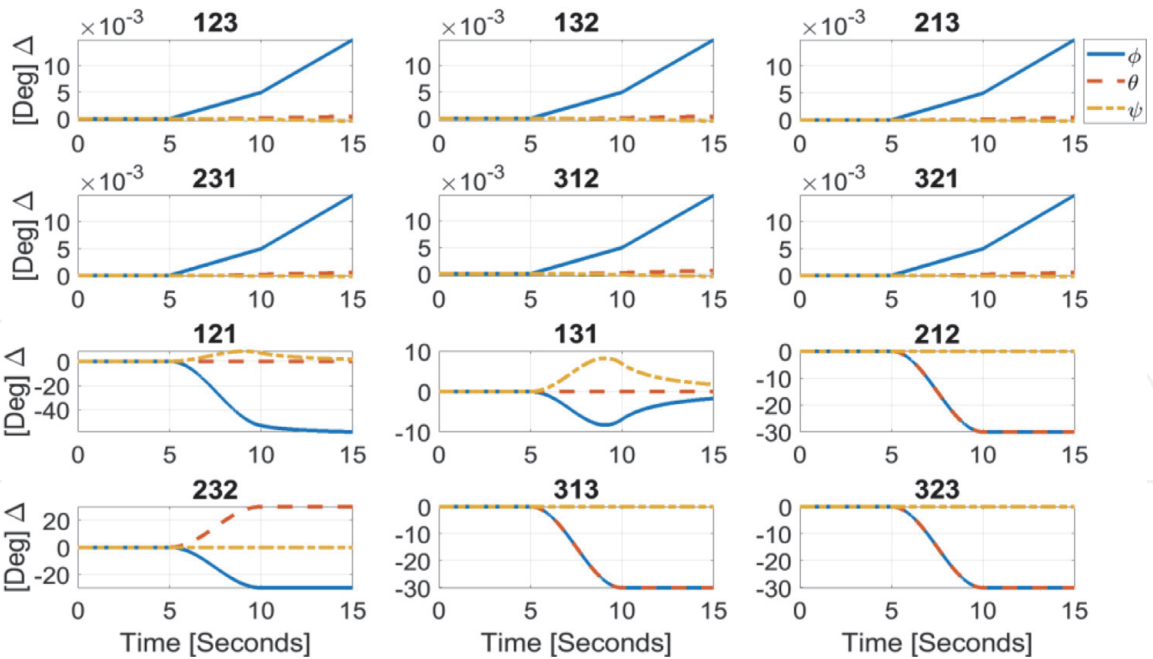


Figure 5.
Euler and body angle deviation, using a 0.001 step size.

DCM	Execution time (s)		
	0.1 step size	0.001 step size	0.0001 step size
1-2-3	8.408	11.836	28.433
1-3-2	1.533	6.789	22.187
2-1-3	1.419	6.978	22.102
2-3-1	1.188	4.436	23.259
3-1-2	1.549	4.302	20.971
3-2-1	1.018	3.475	21.420
1-2-1	0.952	3.715	20.505
1-3-1	1.190	4.082	23.331
2-1-2	1.015	3.860	21.005
2-3-2	0.931	3.710	21.410
3-1-3	0.939	3.789	20.908
3-2-3	1.091	3.955	22.044

Table 2.
Simulation run times for all 12 direction cosine matrices (DCM) rotations for a 30° roll maneuver, using 0.1, 0.001, and 0.0001 step sizes.

different rotations (vertically in the **Table 2**) and not between step sizes (horizontally in **Table 2**); however, relative comparisons between step sizes are valid.

Three observations can be made from the results in **Table 2**. The first is that the slowest rotation is the 1-2-3 rotation, by a significant amount depending upon the step size. The second is that on average, non-symmetric rotations were faster than symmetric rotations. This result is unique because the same algorithm with the same number of mathematical steps yielded different execution times. Lastly, the fastest overall rotation was the 2-3-2 rotation, with 3-2-1 as the fastest non-symmetric rotation.

4. Conclusions

This chapter on modern kinematics or motion phoronomics elaborated all 12 possible instantiations of direction cosine matrices with comparisons of numerical accuracy representing how accurately the chosen Euler angle represents the roll, pitch, and yaw expressions of rotations about x, y, z axes respectively. Additionally, comparison is made by using the figure of merit of computation burden expressed in time-necessary to perform calculations using each respective kinematic instantiation. The results were listed in a large table of options available for trade-offs, where symmetric sequences proved more difficult to compare and correlate, meanwhile the non-symmetric rotational sequences proved easier to correlate to roll, pitch, and yaw due to the ease of allocating independent angles.

The “trade-space” of options is a key elaboration, since none of the options were unanimously best using more than one figure of merit. If accuracy measured by mean error is most relatively important, 1-2-3, 1-3-2, 2-1-3, 2-3-1, 3-1-2, or 3-2-1 rotational sequences best represent roll, while the ubiquitous 3-2-1 sequence cannot best to represent pitch, where the 1-2-3 sequence is superior; while 2-1-3, 2-3-1, and 3-2-1 rotational sequences can most accurately reflect yaw. Instead if accuracy measured by standard deviation of errors was most important, the results were not identical. The most computationally efficient rotational sequence was the 2-3-2 rotation, while the 3-1-3 and 1-2-1 performed next in the list of best options. Oddly, the ubiquitous 3-2-1 sequence was merely the fifth fastest option.

The demonstration of relative inferiority of the standard ubiquitous options is a key novel development in the chapter, and the novelties were validated using a relatively high fidelity simulation of spacecraft attitude dynamics, but the novel development are valid for other forms of rotational motion mechanics like naval vessels, airplanes, and even robotics.

Future works will validate these results on laboratory spacecraft hardware simulators at the Naval Postgraduate School, and if successful flight in space is available on the international space station making the technology available to enhance the aforementioned applications of the technology [35–45].

Acknowledgements

We would like to thank our teacher, Dr. Timothy Sands for his guidance in developing this work, as well as our families for their support while we spent our time away from them developing this research, so thank you.

Conflict of interest

The authors declare no conflict of interest.

IntechOpen


IntechOpen

Author details

Brendon Smeresky* and Alex Rizzo
Naval Postgraduate School Monterey, California, United States

*Address all correspondence to: bpsmeres@nps.edu

IntechOpen

© 2020 The Author(s). Licensee IntechOpen. Distributed under the terms of the Creative Commons Attribution - NonCommercial 4.0 License (<https://creativecommons.org/licenses/by-nc/4.0/>), which permits use, distribution and reproduction for non-commercial purposes, provided the original is properly cited. 

References

- [1] Euler L. (Euler) *Formulae Generales pro Translatione Quacunque Corporum Rigidorum* (General Formulas for the Translation of Arbitrary Rigid Bodies), Presented to the St. Petersburg Academy on 9 October 1775. and First Published in *Novi Commentarii Academiae Scientiarum Petropolitanae* 20, 1776, pp. 189–207 (E478) and Was Reprinted in *Theoria motus corporum rigidorum*, ed. nova, 1790, pp. 449–460 (E478a) and Later in His Collected Works *Opera Omnia*, Series 2, Volume 9, pp. 84–98. Available from: <https://math.dartmouth.edu/~euler/docs/originals/E478.pdf> [Accessed: August 22, 2018]
- [2] Thompson W, Tait PG. *Elements of Natural Philosophy*. Cambridge, UK: Cambridge University Press; 1872
- [3] Reuleaux F, Kennedy Alex BW. *The Kinematics of Machinery: Outlines of a Theory of Machines*. London, UK: Macmillan; 1876. Available from: <https://archive.org/details/kinematicsofmach00reuluoft> [Accessed: August 22, 2018]
- [4] Wright TW. *Elements of Mechanics Including Kinematics, Kinetics and Statics*. New York, NY, USA/ Cambridge, MA, USA: D. Van Nostrand Company/Harvard University; 1896
- [5] Merz JT. *A History of European Thought in the Nineteenth Century*. London, UK: Blackwood; 1903. p. 5
- [6] Whittaker ETA. *Treatise on the Analytical Dynamics of Particles and Rigid Bodies*. Cambridge, UK: Cambridge University Press; 1904
- [7] Whittaker ET. *A Treatise on the Analytical Dynamics of Particles and Rigid Bodies*. Cambridge, UK: Cambridge University Press; 1917
- [8] Whittaker ET. *A Treatise on the Analytical Dynamics of Particles and Rigid Bodies*. Cambridge, UK: Cambridge University Press; 1927
- [9] Whittaker ET. *A Treatise on the Analytical Dynamics of Particles and Rigid Bodies*. Cambridge, UK: Cambridge University Press; 1937
- [10] Church IP. *Mechanics of Engineering*. New York, NY, USA: Wiley; 1908. p. 111
- [11] Wright TW. *Elements of Mechanics Including Kinematics, Kinetics, and Statics, with Applications*. New York, NY, USA: Nostrand; 1909
- [12] Study E, Delphenich DH. Foundations and goals of analytical kinematics. *Sitzber. d. Berl. Math. Ges.* 1913;**13**:36–60. Available from: http://neo-classical-physics.info/uploads/3/4/3/6/34363841/study-analytical_kinematics.pdf [Accessed: April 14, 2017]
- [13] Gray A. *A Treatise on Gyrostatics and Rotational Motion*. London, UK: MacMillan; 1918. ISBN: 978-1-4212-5592-7 (Published 2007)
- [14] Rose ME. *Elementary Theory of Angular Momentum*. New York, NY, USA: John Wiley & Sons; 1957. ISBN: 978-0-486-68480-2 (Published 1995)
- [15] Kane TR. *Analytical Elements of Mechanics*. Vol. 1. New York, NY, USA/ London, UK: Academic Press; 1959
- [16] Kane TR. *Analytical Elements of Mechanics*. Vol. 2: Dynamics. New York, NY, USA/London, UK: Academic Press; 1961
- [17] Thompson W. *Space Dynamics*. New York, NY, USA: Wiley and Sons; 1961

- [18] Greenwood D. Principles of Dynamics. Englewood Cliffs, NJ, USA: Prentice-Hall; 1965. ISBN: 9780137089741 (Reprinted in 1988 as 2nd ed.)
- [19] Fang AC, Zimmerman BG. Digital Simulation of Rotational Kinematics; NASA Technical Report NASA TN D-5302. Washington, DC, USA: NASA; 1969. Available from: <https://ntrs.nasa.gov/archive/nasa/casi.ntrs.nasa.gov/19690029793.pdf> [Accessed: August 22, 2018]
- [20] Henderson DM. Euler Angles, Quaternions, and Transformation Matrices—Working Relationships; As NASA Technical Report NASA-TM-74839. 1977. Available from: <https://ntrs.nasa.gov/archive/nasa/casi.ntrs.nasa.gov/19770024290.pdf> [Accessed: August 22, 2018]
- [21] Henderson DM. Euler Angles, Quaternions, and Transformation Matrices for Space Shuttle Analysis; Houston Astronautics Division as NASA Design Note 1.4-8-020. 1977. Available from: <https://ntrs.nasa.gov/archive/nasa/casi.ntrs.nasa.gov/19770019231.pdf> [Accessed: August 22, 2018]
- [22] Goldstein H. Classical Mechanics. 2nd ed. Boston, MA, USA: Addison-Wesley; 1981
- [23] Kane T, David L. Dynamics: Theory and Application. New York, NY, USA: McGraw-Hill; 1985
- [24] Hughes P. Spacecraft Attitude Dynamics. New York, NY, USA: Wiley and Sons; 1986
- [25] Wiesel W. Spaceflight Dynamics. 2nd ed. Boston, MA, USA: Irwin McGraw-Hill; 1989. p. 1997
- [26] Wie B. Space Vehicle Dynamics and Control. Reston, VA, USA: AIAA; 1998
- [27] Slabaugh GG. Computing Euler Angles from a Rotation Matrix. Vol. 6. 1999. pp. 39-63. Available from: http://www.close-range.com/docs/Computing_Euler_angles_from_a_rotation_matrix.pdf [Accessed: August 22, 2018]
- [28] Vallado D. Fundamentals of Astrodynamics and Applications. 2nd ed. El Segundo, CA, USA: Microcosm Press; 2001
- [29] Roithmayr CM, Hodges DH. Dynamics: Theory and Application of Kane's Method. New York, NY, USA: Cambridge University Press; 2016
- [30] Sands T. Satellite electronic attack of enemy air defenses. In: Proceedings of the IEEE CDC; 2009. pp. 434-438. DOI: 10.1109/SECON.2009.5174119
- [31] Sands T. Space mission analysis and design for electromagnetic suppression of radar. International Journal of Applied Electromagnetics. 2018;8:1-25. DOI: 10.5923/j.ijea.20180801.01
- [32] Sands T, Lu D, Chu J, Cheng B. Developments in angular momentum exchange. International Journal of Aerospace Engineering. 2018;6:1-7. DOI: 10.5923/j.aerospace.20180601.01
- [33] Sands TA, Kim JJ, Agrawal B. 2H singularity free momentum generation with non-redundant control moment gyroscopes. In: Proceedings of the IEEE CDC; 2006. pp. 1551-1556. DOI: 10.1109/CDC.2006.377310
- [34] Sands T. Fine pointing of military spacecraft [PhD dissertation]. Monterey, CA, USA: Naval Postgraduate School; 2007
- [35] Kim JJ, Sands T, Agrawal BN. Acquisition, tracking, and pointing technology development for bifocal relay mirror spacecraft. Proceedings of SPIE. 2007;6569:656907. DOI: 10.1117/12.720694

- [36] Sands TA, Kim JJ, Agrawal B. Control moment gyroscope singularity reduction via decoupled control. In: Proceedings of the IEEE SEC; 2009. pp. 1551-1556. DOI: 10.1109/SECON.2009.5174111
- [37] Sands T, Kim JJ, Agrawal BN. Nonredundant single-gimbaled control moment gyroscopes. *Journal of Guidance, Control, and Dynamics*. 2012; 35:578-587. DOI: 10.2514/1.53538
- [38] Sands T, Kim J, Agrawal B. Experiments in control of rotational mechanics. *International Journal of Automation, Control and Intelligent Systems*. 2016;2:9-22. ISSN: 2381-7534
- [39] Agrawal BN, Kim JJ, Sands TA. Method and apparatus for singularity avoidance for control moment gyroscope (CMG) systems without using null motion. U.S. Patent 9567112 B1; 2017. Available from: <https://calhoun.nps.edu/handle/10945/51921> [Accessed: August 22, 2018]
- [40] Sands T, Kim JJ, Agrawal B. Singularity penetration with unit delay (SPUD). *Mathematics*. 2018;6:23. DOI: 10.3390/math6020023. Available from: <http://www.mdpi.com/2227-7390/6/2/23/pdf> [Accessed: August 22, 2018]
- [41] Nakatani S, Sands T. Simulation of spacecraft damage tolerance and adaptive controls. In: Proceedings of the IEEE Aerospace Conference; 2014. pp. 1-16. DOI: 10.1109/AERO.2014.6836260
- [42] Nakatani S, Sands T. Autonomous damage recovery in space. *Int. J. Autom. Control Intell. Syst.* 2016;2:22-36. ISSN: 2381-75
- [43] Nakatani S, Sands T. Battle-damage tolerant automatic controls. *Journal of Electrical and Electronic Engineering*. 2018;8:10-23. DOI: 10.5923/j.eee.20180801.02
- [44] Sands T, Mihalik R. Outcomes of the 2010 and 2015 nonproliferation treaty review conferences. *World Journal of Social Science*. 2016;2:46-51. DOI: 10.12691/wjssh-2-2-4. Available online at: <http://pubs.sciepub.com/wjssh/2/2/4/index.html> [Accessed: August 22, 2018]
- [45] Sands T. Strategies for combating Islamic state. *Social Science*. 2016;5: 39-39. DOI: 10.3390/socsci5030039. Available from: www.mdpi.com/2076-0760/5/3/39/pdf [Accessed: August 22, 2018]
- [46] Mihalik R, Camacho H, Sands T. Continuum of learning: Combining education, training and experiences. *Education*. 2017;8:9-13. DOI: 10.5923/j.edu.20180801.03
- [47] Sands T, Camacho H, Mihalik R. Education in nuclear deterrence and assurance. *Journal of Defense Studies and Resource Management*. 2017;7: 166-166. DOI: 10.4172/2167-0374.1000166
- [48] Sands T, Mihalik R. Theoretical context of the nuclear posture review. *Journal of Social Sciences*. 2018;14: 124-128. DOI: 10.3844/jssp.2018.124.128. Available from: <http://thescipub.com/pdf/10.3844/jssp.2018.124.128> [Accessed: August 22, 2018]
- [49] Sands T, Lorenz R. Physics-based automated control of spacecraft. In: Proceedings of the AIAA Space 2009 Conference and Exposition; Pasadena, CA, USA; 14–17 September 2009
- [50] Sands T. Physics-Based Control Methods. In *Advances in Spacecraft Systems and Orbit Determination*. London, UK: InTechOpen; 2012. DOI: 10.5772/2408. Available from: <https://www.intechopen.com/books/advances-in-spacecraft-systems-and-orbit-determination/physics-based-control-methods> [Accessed: August 22, 2018]

- [51] Sands T. Improved magnetic levitation via online disturbance decoupling. *Physik Journal*. 2015;1: 272-280
- [52] Heidlauf P, Cooper M. Nonlinear Lyapunov control improved by an extended least squares adaptive feed forward controller and enhanced Luenberger observer. In: *Proceedings of the International Conference and Exhibition on Mechanical & Aerospace Engineering*; Las Vegas, NV, USA; 2–4 October 2017
- [53] Cooper M, Heidlauf P, Sands T. Controlling chaos—Forced van der pol equation. *Mathematics*. 2017;5:70. DOI: 10.3390/math5040070. Available from: <http://www.mdpi.com/2227-7390/5/4/70/pdf> [Accessed: August 22, 2018]
- [54] Sands T. Phase lag elimination at all frequencies for full state estimation of spacecraft attitude. *Physik Journal*. 2017;3:1-12
- [55] Sands T. Nonlinear-adaptive mathematical system identification. *Computation*. 2017;5:47-59. DOI: 10.3390/computation5040047. Available online at <http://www.mdpi.com/2079-3197/5/4/47/pdf> [Accessed: August 22, 2018]
- [56] Sands T, Kenny T. Experimental piezoelectric system identification. *Journal of Mechanical Engineering and Automation*. 2017;7:179-195. DOI: 10.5923/j.jmea.20170706.01
- [57] Sands T. Space systems identification algorithms. *Journal of Space Exploration*. 2017;6:138-149. ISSN: 2319-9822
- [58] Sands T. Experimental sensor characterization. *Journal of Space Exploration*. 2018;7:140. Available from: <https://www.tsijournals.com/articles/experimental-sensor-characterization-13620.html>. [Accessed: August 22, 2018]
- [59] Sands T, Armani C. Analysis, correlation, and estimation for control of material properties. *Journal of Mechanical Engineering and Automation*. 2018;8:7-31. DOI: 10.5923/j.jmea.20180801.02. Available from: <http://www.sapub.org/global/showpaperpdf.aspx?doi=10.5923/j.jmea.20180801.02> [Accessed: August 22, 2018]
- [60] Sands T. Satellite electronic attack of enemy air defenses. In: *Proceedings of the IEEE SEC*; Atlanta, GA, USA; 5–8 March 2009. pp. 434-438
- [61] Remarks by President Trump at a Meeting with the National Space Council and Signing of Space Policy Directive-3. Available from: <https://www.whitehouse.gov/briefings-statements/remarks-president-trump-meeting-national-space-council-signing-space-policy-directive-3/> [Accessed: June 20, 2018]
- [62] Sands T, Bollino K, Kaminer I, Healey A. Autonomous minimum safe distance maintenance from submersed obstacles in ocean currents. *Journal of Marine Science and Engineering*. 2018; 6:98. Available from: <http://www.mdpi.com/2077-1312/6/3/98/pdf> [Accessed: August 22, 2018]
- [63] Kuipers JB. *Proceedings of the Quaternions and Rotation Sequences, Geometry, Integrability, and Quantization*, Varna, Bulgaria, 1–10 September 1999. Sofia, Bulgaria: Coral Press; 2000
- [64] Sands T. Optimization provenance of whiplash compensation for flexible space robotics. *Aerospace*. 2019;6:93
- [65] Sands T. Comparison and interpretation methods for predictive control of mechanics. *Algorithms*. 2019; 12:232